Research article

Dong Hyeon Kim, Chanwoo Lee, Byeong Geun Jeong, Sung Hyuk Kim and Mun Seok Jeong*

Fabrication of highly uniform nanoprobe via the automated process for tip-enhanced Raman spectroscopy

https://doi.org/10.1515/nanoph-2020-0210
Received March 26, 2020; accepted May 6, 2020

Abstract: In a tip-enhanced Raman spectroscopy (TERS) system, using a sharp nanotip that comprises a noble metal is critical to attaining high spatial resolution and highly enhanced Raman scattering. A strongly acidic solution is typically used to fabricate gold nanotips in a quick and reliable manner. However, using an acidic solution could corrode the etching system, thereby posing hazardous problems. Therefore, both the corrosion of the etching system and human error induced by the conventional method considerably decrease the quality and reproducibility of the tip. In this study, we significantly increased the reproducibility of tip fabrication by automating the electrochemical etching system. In addition, we optimized the etching conditions for an etchant that comprised a KCl solution to which ethanol was added to overcome the limitations of the acidic etchant. The automated etching system significantly increases the yield rate of tip-fabrication reproducibility from 65 to 95%. The standard deviation of the radius of curvature decreased to 7.3 nm with an average radius of curvature of 30 nm. Accordingly, the automated electrochemical etching system might improve the efficiency of TERS.

KEYWORDS: automation; electrochemical etching; non-acidic etchant; tip-enhanced Raman spectroscopy (TERS); tip fabrication.

1 Introduction

Gold (Au) is widely used as the probe material in tip-enhanced Raman spectroscopy (TERS) because of its stable chemical characteristics under ambient conditions compared with other materials. TERS is a nanoscale spectroscopic technique that is used in combination with scanning probe microscopy and confocal Raman spectroscopy [1–6]. Accordingly, fabricating a sharp nanotip is critical to improving the spatial resolution of a TERS image. TERS, which is a powerful tool, not only produces Raman scattering images with high spatial resolution but also has a significantly enhanced Raman signal, thereby enabling various low-dimensional materials to be investigated [7–10]. A sharp Au tip can be implemented as both a probe for scanning probe microscopy and a source of near-field light, owing to the localized surface plasmon resonance (LSPR). This resonance is attributed to the high density of free electrons in Au, which significantly increases the electric-field intensity near the surface of the tip apex [11–13]. Therefore, the ability to produce sharp-edged Au nanotips with a controlled smooth shape and yield rate is critical to performing TERS-based studies.

Thus far, various methods, such as mechanical shaping [14–16], ion beam milling [17, 18], chemical polishing [19], template stripping [20], and electrochemical etching [21–23], have been developed to fabricate Au nanotips. Particularly, most research groups have been using electrochemical etching because it offers several advantages as follows: low fabrication cost [18, 21], reliable tip quality [24–26], and simple manufacturing procedure [22, 23]. However, they typically used a strong acid, such as HCl or H_2SO_4, as an etchant to fabricate the tips. The problems due to the hazardous nature of the etchants have not still been solved. In addition, strongly acidic vapors corrode the electrochemical etching system, thereby introducing significant errors during tip fabrication. Nevertheless, the research on non-acidic etchants is not only scarce but has also shown a reduction in the quality of the etched tip [21, 27]. Furthermore, an STM probe was

Dong Hyeon Kim and Chanwoo Lee: The authors are equally contributed.

***Corresponding author: Mun Seok Jeong**, Department of Energy Science, Sungkyunkwan University, Suwon 16419, Republic of Korea, E-mail: mjeong@skku.edu
Dong Hyeon Kim, Chanwoo Lee, Byeong Geun Jeong and Sung Hyuk Kim: Department of Energy Science, Sungkyunkwan University, Suwon 16419, Republic of Korea, E-mail: dong6882@gmail.com (D.H. Kim), Chanwoo@skku.edu (C. Lee), zinzza228@gmail.com (B.G. Jeong), sh.kim@skku.edu (S.H. Kim)

fabricated only recently using a three-electrode method and KCl-based etchant [28]. In addition, the reproducibility of the tips that have been fabricated via the electrochemical etching method still remains problematic and has not still been resolved. Ultimately, the human error due to using the conventional method is the main reason for the decrease in the reliability of tip fabrication, thereby necessitating the automation of the fabrication system. As much as it is currently important to investigate various materials by using TERS, research to improve the reproducibility of sharp-tip fabrication is equally critical to increasing the performance efficiency of TERS.

In this study, we optimized the electrochemical-etching conditions with the aim of fabricating a sharp Au tip for TERS. We used an etchant that comprised a mixture of an aqueous KCl solution, i. e., an inorganic chloride material, and ethanol, to avoid the hazardous and corrosive nature of the etchants. The etching procedure was performed by applying the square-wave voltage to an Au wire and a platinum (Pt) ring, both of which acted as the anode and cathode, respectively. Moreover, we automatized the electrochemical etching system by connecting the devices necessary for etching to highly increase the yield rate, as well as to decrease the variation in the tip parameters; as such variations had previously occurred because of human error. Additionally, we demonstrated the effectiveness of the automatically etched Au tip by measuring a strongly enhanced TERS signal of monolayer WSe_2.

2 Experimental Section

2.1 Preparation of the etchant solution

KCl powder was dissolved in DI water at a concentration of 2.8 mol/L in ambient conditions. A vortex mixer was used to ensure that the KCl powder completely dissolved. Subsequently, the KCl solution was mixed with 99.9% anhydrous ethanol in the volume ratio, i. e., KCl:ethanol, of 4:1. Because the addition of the ethanol resulted in precipitation, the mixture was again shaken using the vortex mixer. Finally, the concentration of the KCl included in the etchant was adjusted by adding DI water (1 mL) to the KCl solution and ethanol mixture (19 mL).

2.2 Electrochemical etching process

Au nanotips were fabricated in optimized etching conditions using a homemade electrochemical etching system. An Au wire (0.1 mm; 99.95%; Nilaco, Japan) and Pt ring (0.2 mm; 99.98%; Nilaco, Japan) acted as the anode and cathode, respectively. The square-wave-pulsed voltage was applied to the Au and Pt electrodes using a waveform generator. The applied electrical conditions were as follows: maximum voltage of 2.417 V, minimum voltage of −250 mV, frequency of 300 Hz, and duty cycle of 77%. The Au nanowire was immersed (up to the depth of 0.1 mm) in 20 mL of the etchant. After the automated etching completed, the etched Au tips were rinsed using four solvents, namely, acetone, ethanol, DI water, and isopropyl alcohol. Finally, an N_2 gun was used to remove the residue from the tips.

2.3 Tip-enhanced Raman scattering measurements

A TERS system comprises an STM and a confocal Raman spectroscope (NTEGRA Spectra, NT-MDT Co., Zelenograd, Russia). The system was used to measure both the confocal Raman scattering and TERS. The measurements were conducted using a 633-nm wavelength laser, and the objective lens used for both the Raman measurements had the numerical aperture of 0.7 and magnification of ×100 (Mitutoyo, Japan). The confocal Raman scattering signal and TERS signal were obtained for 10 s using a charge-coupled device (Andor, UK), which was cooled to −76 °C and had a grating with 1800 grooves/mm, blazed at 500 nm.

3 Results and discussion

The sharp Au tips for the TERS measurement were fabricated via electrochemical etching by using the homemade etching system. This system is depicted in Figure 1. From the figure, it is evident that the Au wire and Pt ring are connected to the positive and negative poles of the waveform generator, respectively, such that the Au wire becomes the anode. The Pt ring, which serves as the cathode, is immersed in the etchant near the surface of the solution. In addition, the Au wire is immersed in the center of the Pt ring up to the depth of 0.1 mm. The height of the Au wire was adjusted using the stepper motorized actuator, which was controlled via the stepper controller. As depicted in Figure 1, all the devices, such as the stepper controller and waveform generator, are connected to the computer to automate the electrochemical etching process.

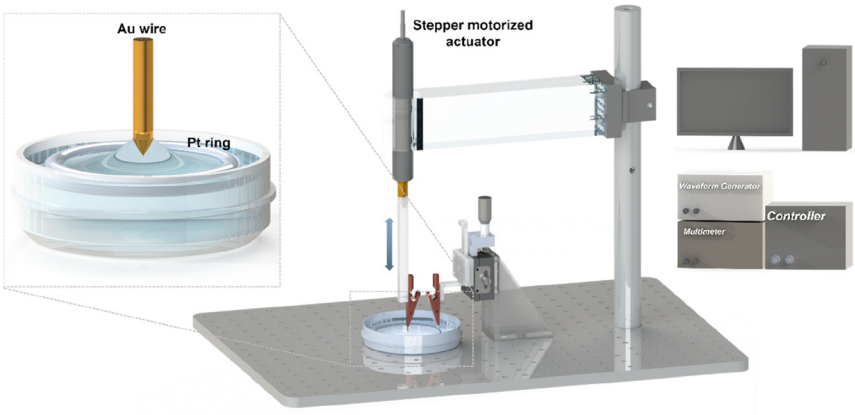

Figure 1: Electrochemical etching system. Homemade electrochemical etching system. The enlarged illustration represents the electrochemical etching process with bias applied. The stepper motorized actuator, stepper controller, waveform generator, and multimeter are connected to a computer to automate the electrochemical etching process.

The Au etching reaction mainly occurs at the meniscus of the etchant around the Au wire and is expressed as follows [21–29]:

$$Au_{(s)} + 4Cl^-_{(aq)} \rightarrow [AuCl_4]^-_{(aq)} + 3e^-$$
$$Au_{(s)} + 2Cl^-_{(aq)} \rightarrow [AuCl_2]^-_{(aq)} + e^-$$

In both above-mentioned equations, the chloride ion is the key element to electrochemically etching the Au wire. During the etching process, Au becomes unstable and dissolves in the solution, which mainly contains chloride ions [29]. Therefore, an alternative for the conventional etchant must be a chlorine-containing compound, such as an HCl solution. Accordingly, various chlorine-containing inorganic-salt candidates, such as LiCl, NaCl, KCl, and $CaCl_2$, which would not corrode the etching system, can be used as the new etchant material. First, we examined the solubility value of the candidates to estimate the amount of chloride ions in the etchant solution. Although LiCl and $CaCl_2$ have higher solubilities than those of NaCl and KCl at approximately 20 °C [30], they could irritate the central nervous system of humans [31, 32]. In addition, their solubility significantly varies with temperature [30], thereby easily affecting the etching conditions. Although the chemical properties of NaCl are similar to those of KCl, the average etching time using 3 M NaCl without acid was approximately 1900 s [33]. Therefore, instead of using a strong acid or the solutions of other inorganic salts, we decided to use an aqueous solution of KCl as the electrochemical etchant to effectively fabricate the TERS tip.

We optimized the etching condition of the Au wire before automating the etching system. Many factors influence the shape of an etched tip (e. g., the etchant concentration, volume ratio of ethanol to the etchant, applied bias potential, duty cycle, and immersion depth of the Au wire). Especially, the etchant concentration and the bias potential primarily determine the radius of the tip apex (R_{tip}), cone angle, and etching time. The application of high potential results in a strong current, affecting the cone angle and shape of the etched tip [21, 24–26]. In addition, the duty cycle is crucial to prevent the cut-off of the electrochemical etching circuit by the insulating layer around the Au wire [18]. The immersion depth of the wire also slightly affects the etched tip.

First, the concentration of the aqueous KCl solution was adjusted. The amount of chloride ions in the conventional HCl solution as etchant is significantly higher than that in the conventional KCl solution; therefore, the KCl solution should be prepared by dissolving as much KCl in deionized (DI) water as possible until the solubility limit is reached. The chloride ions are crucial for the etching process, as the abundance of chloride ions can significantly accelerate the etching speed. The water solubility of KCl at approximately 20 °C is approximately 36 g/100 g H_2O [30]. However, during the etching process performed using this saturated solution, KCl precipitated throughout the etchant. This precipitation is undesirable, as the KCl precipitate could interrupt the behavior of several ions and also decrease the current flow by acting as an insulating layer. Furthermore, the solubility of KCl in ethanol is extremely low and could again result in a precipitation-related issues. Therefore, we adjusted the concentration of the aqueous solution of KCl to 2.8 M via experimentation.

We added ethanol to the etchant during the etching process to smooth the surface of the etched tip and control the etching speed. Accordingly, we optimized the volume ratio of the KCl solution to ethanol by conducting experiments with the peak amplitude of 3.5 V, background value of −250 mV, frequency of 300 Hz, and duty cycle of 80%. The results are depicted in Figure 2b-d. In addition, we compared the shape and parameters associated with the tip by capturing representative field emission scanning

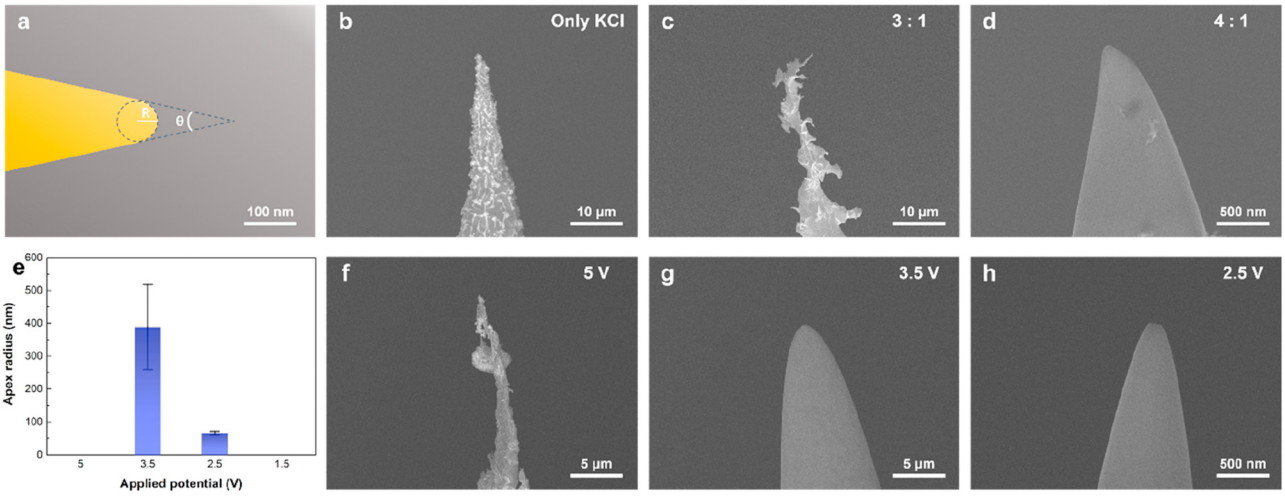

Figure 2: Electrochemically etched Au tips with different etchants and applied potential. (a) The Au-tip model, which shows the radius of curvature R and cone angle θ. (b–d) The field emission scanning electron microscopy (FE-SEM) images of Au tips with different volume ratios of KCl solution to ethanol. (Ethanol free, 3:1, and 4:1, respectively; 3.5 V was applied with an 80% duty cycle.) (e) The dependence of the average tip radius on the applied potential. (f–h) The FE-SEM images of Au tips with different applied potentials. (5, 3.5, and 2.5 V, respectively, with an 80% duty cycle.)

electron microscopy images of the etched Au tips, as depicted in Figure 2. The radii of curvature and cone angles of all the tips were measured, as shown in Figure 2a. When only the KCl solution was used, as illustrated in Figure 2b, the shape of the etched tip resembled that of a needle-leaf tree and was inappropriate for the TERS experiments. Moreover, using KCl solution and ethanol in the ratios 1:1 and 2:1 resulted in a precipitation-related problem (the corresponding SEM images are not included in Figure 2). When the ratio was 3:1, the resulting tip was tree-shaped and could not be used. The ratio of 4:1 yielded a sharp tip (see Figure 2d); however, upon increasing the volume ratio of the KCl solution, the shape of the etched tip changed into the shape that is obtained using only the KCl solution.

Similar to the etchant conditions, the potential bias applied for performing electrochemical etching is also considered a significant factor. To investigate the extent to which the shape depends on the potential bias, we performed electrochemical etching by using the volume ratio of 4:1 (see Figure 2f–h) while maintaining the other conditions the same as those for the other volume-ratio-dependence etching experiments. The SEM images of the Au tips etched using various applied potentials are depicted in Figure 2f–h. In addition, Figure 2e depicts an integrated histogram that shows the dependence of the tip-apex radius on the applied potential. Upon applying the potential bias of 5 V, an irregularly and roughly shaped etched tip is produced, as depicted in Figure 2f. Although the tip fabricated using the potential bias of 3.5 V has a sharp apex (see Figure 2g), its radius is estimated to be approximately 400 nm. Upon applying the potential bias of 2.5 V, the average R_{tip} was approximately 70 nm. Although the radius was close to that required for TERS experiments, the yield rate was undesirably low. The result obtained upon applying the potential bias of 1.5 V is excluded from Figure 2 because at this bias, more than 15 min are required to obtain one Au nanotip.

The etching conditions must be optimized by conducting more accurate TERS experiments to reduce the average R_{tip} to less than 50 nm. As depicted in Figure 3a-e, we performed electrochemical etching by adjusting the potential bias in minute steps. The average tip-apex radii for five potential conditions are plotted in Figure 3a, in which the error bars represent the standard deviation. Figure 3b–e depict the representative SEM images, and the radius of curvature and cone angle of each tip correspond to the applied potential. The Au tip was fabricated using the same conditions as those in Figure 2e, except for the bias potential. As depicted in Figure 3a–e, the average R_{tip} decreases upon decreasing the potential bias from 2.450 to 2.417 V. In addition, the etched tip with the smallest radius of approximately 37 nm was fabricated by applying the bias voltage of 2.417 V.

After adjusting the electrical conditions for the etching process, we minutely modulated the etchant conditions. This is because the initial experiments in which the etchant conditions were varied were performed prior to optimizing the electrical-etching conditions. Furthermore, because the nanoscale dimensions of the TERS tip apex are significantly affected by both etching and environmental

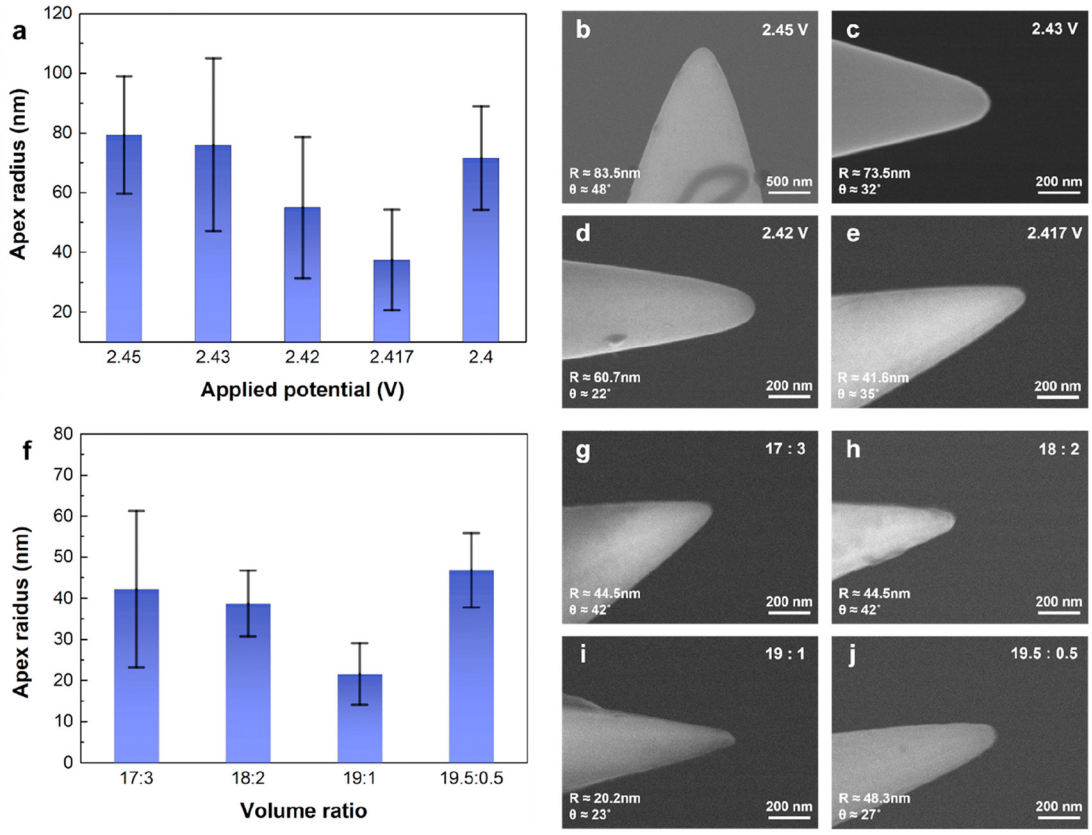

Figure 3: Electrochemically etched Au tips fabricated in optimized etching conditions. (a) The dependence of the average tip radius on the applied potential. (b–e) The FE-SEM images of Au tips at various applied potentials. (2.450, 2.430, 2.420, and 2.417 V, respectively, with an 80% duty cycle.) (f) The dependence of the average tip radius on the volume ratio. (g–j) The FE-SEM images of Au tips at various etchant/DI-water volume ratios. (17:3, 18:2, 19:1, and 19.5:0.5, respectively. In addition, 2.417 V was applied with a 77% duty cycle.)

conditions, these conditions had to be precisely optimized. Accordingly, we controlled the etchant concentration by adding DI water to the etchant, as depicted in Figure 2d. Furthermore, as depicted in Figure 3f, the following four volume ratios of the etchant to DI water were employed: 17:3, 18:2, 19:1, and 19.5:0.5, respectively. The SEM images of the tips fabricated in these etchant conditions are depicted in Figure 3g-j with the corresponding parameters. For the volume ratio of 19:1 between the mixture of the etchant and DI water, we successfully fabricated a tip whose minimum average apex radius was approximately 20 nm, as depicted in Figure 3f. Electrochemical etching was conducted using the same electrical conditions as those in Figure 3a, except for the duty cycle of 77%.

To optimize the electrochemical etching system, the conversion of the working process from the established system that is currently being used is critical to overcoming the limitation due to human error. Notably, the most significant problem of the previous system is the absence of objective criteria at each step of the etching procedure. First, to reduce the deviations in the R_{tip}, the wire must be lowered by exactly the same depth each time the Au tip is fabricated. Second, to prevent the Au wire from being over-etched, the potential bias should be immediately discontinued once the etching has finished. Third, although the etched tips are rinsed using acetone, ethanol, DI water, and isopropyl alcohol after etching, the Au tip should be promptly raised to avoid contamination by the precipitate. Avoiding the precipitate-induced contamination in the etching process is important, as the contamination can disturb the formation of LSPR and subsequently diminish the Raman-signal enhancement.

Figure 4a depicts the connections between the different components of the electrochemical etching system. The waveform generator, multimeter, and stepper controller are connected with the computer, and the stepper motorized actuator is connected only with the stepper controller. The computer gathers information of the electrical parameters, such as current and voltage, as a function of time and then controls the waveform generator and the stepper controller by employing the current value that was previously attained. The workflow of this etching

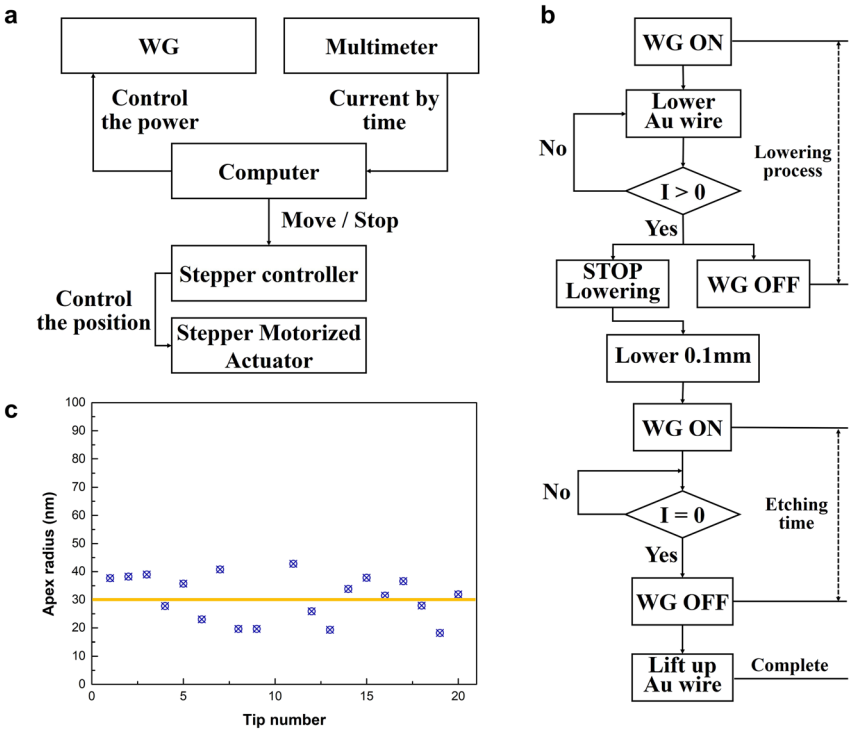

Figure 4: Algorithms of automated etching system and histogram for the tips fabricated using this system. (a) The electrochemical-etching equipment in the system and the connections among the components. (b) The workflow of the electrochemical etching system. (c) Scatter diagram that depicts the variations in the R_{tip}. The yellow solid line represents the average radius value.

system comprises the following three operations: lowering, etching, and returning to the start position, as depicted in Figure 4b. To ensure that the immersion depth of each Au wire is the same, we must fix the starting point of the lowering step. Once the Au wire starts touching the surface of the etchant with the bias applied, the current rapidly increases to over 0.8 mA. In addition, to avoid pre-etching, the computer discontinues the applied bias and prevents the tip from moving as soon as the etching operation is complete. After lowering the wire by 0.1 mm, the electrochemical etching of the wire begins by implementing the previously optimized conditions provided in Figure 3. Upon the completion of the etching operation, the value of the current decreases to zero because the Au tip is separated from the etchant (short circuit in Figure 4b), and the waveform generator immediately shuts down. Finally, the etched Au tip is lifted to the starting position before being lowered.

To confirm that the automated system is satisfactorily designed, we verified the accuracy and precision of this system by measuring the radius of the tip apex (see Figure 4c). Before installing the automated etching system, the criterion for calculating the yield rate of the fabricated TERS tip is the apex radius of 100 nm. Based on this criterion, the yield rate shown in Figure 3i is approximately 65%, whereas the yield rate increases to 90% for the criterion value of 50 nm and 99% for the criterion value of 100 nm for this automated etching system. The standard deviation of the R_{tip} is 7.3 nm, which is substantially lower than that in the previous value. Therefore, we demonstrated that one can fabricate TERS tips in a precise and safe manner under the optimized conditions by eliminating human errors.

Sharp Au nanotips were fabricated to enhance the Raman scattering signal in the TERS experiment. We assessed the performance of the Au tip fabricated using the electrochemical etching system to confirm the TERS enhancement. As depicted in Figure 5a, a monolayer WSe_2 flake on an Au substrate was measured using a He–Ne laser with the wavelength of 633 nm. The Raman spectra were obtained at the same position on the flake by using confocal Raman scattering (without the tip) and TERS (with the tip) to determine the contrast in the enhancement factor between the Raman spectra and TERS. The LSPR of the gold nanotip caused the WSe_2 to exhibit many peaks, which would not have been possible to distinguish via confocal Raman microscopy. To calculate the contrast value and enhancement factor, the intensities of the 2LA(M) peaks at approximately 260 cm^{-1} on the TERS spectrum (blue solid line) were compared with those on the confocal Raman spectrum (black solid line), as depicted in Figure 5b. The contrast value can be determined by obtaining the intensity ratio of both the 2LA(M) peaks depicted in Figure 5b, and the value of the TERS enhancement factor can be calculated using the obtained contrast value, radius of the laser spot, and measured R_{tip}. The defined equations for

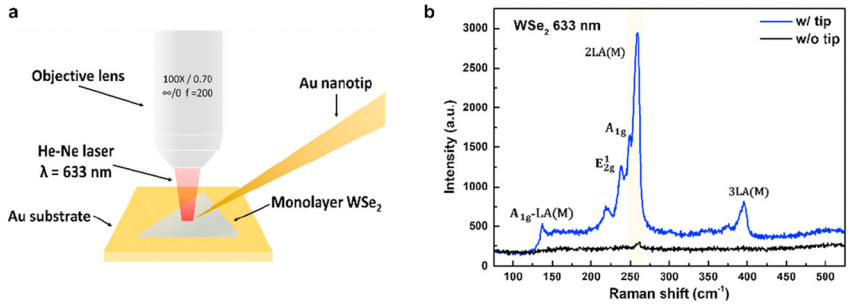

Figure 5: TERS spectra of monolayer WSe_2 when using a tip fabricated using the homemade etching system and the harmless etchant. (a) Schematic illustration of TERS experiment. (b) TERS spectrum (blue curve) and confocal Raman spectrum (black curve) measured at the same position on the WSe_2 sample.

both the contrast and enhancement factor are represented as follows [7, 22, 34]:

$$Contrast = \frac{I_{with\ tip} - I_{without\ tip}}{I_{without\ tip}}$$

$$EF_{TERS} = Contrast \times \left(\frac{R_{laser}}{R_{tip}}\right)^2$$

Here, the Au tip depicted in Figure 3i was used to conduct the TERS experiment and calculate the contrast value and enhancement factor. The apex radius of the used tip is approximately 20.2 nm. The contrast value of the 2LA(M) peak is calculated to be approximately 21.26, and the radius of the excitation laser spot is approximately 550 nm. When using these values, the TERS enhancement factor calculated using the second equation is approximately 22,253. These results indicate that the automated electrochemical etching system, which was optimized by adjusting both the electrical parameters and the concentration of the KCl-containing etchant, facilitates the effective fabrication of a TERS Au tip. Furthermore, we demonstrated that the Au tip etched using the automated system enhanced the intensity of the Raman scattering signal. Accordingly, the automated etching system can be distinctly used for TERS studies.

4 Conclusion

An electrochemical etching system for fabricating sharp Au tips was automated and modified for use with a noncorrosive and nontoxic etchant. The conditions for nanotip fabrication using the KCl-solution-based etchant were experimentally determined. The automation of the electrochemical etching process markedly increased the yield rate at which a tip can be fabricated, from approximately 65 to 95%, and the standard deviation of the apex radius remarkably decreased while maintaining the cost-effectiveness of the electrochemical etching process. Moreover, we demonstrated the performance of the optimized system by acquiring a highly enhanced Raman signal of monolayer WSe_2 with the contrast value of 21.26 and enhancement factor of 22,253 for the 2LA(M) peak when using a tip that was fabricated using the automated etching system.

Acknowledgments: This research was supported by the National Research Foundation of Korea (NRF) grant funded by the Korean government's Ministry of Science and ICT (MSIT) (NRF-2019M3D1A1078304 and NRF-2019R1A2B5B02070657).
Author contribution: All the authors have accepted responsibility for the entire content of this submitted manuscript and approved submission.
Research funding: None declared.
Employment or leadership: None declared.
Honorarium: None declared.
Conflict of interest statement: The authors declare no conflicts of interest regarding this article.

References

[1] R. M. Stöckle, Y. D. Suh, V. Deckert, and R. Zenobi, "Nanoscale chemical analysis by tip-enhanced Raman spectroscopy," *Chem. Phys. Lett.*, vol. 318, pp. 131–136, 2000.
[2] J.-H. Zhong, X. Jin, L. Meng, et al., "Probing the electronic and catalytic properties of a bimetallic surface with 3 nm resolution," *Nat. Nanotechnol.*, vol. 12, pp. 132–136, 2017.
[3] J. Lee, K. T. Crampton, N. Tallarida, and V. A. Apkarian, "Visualizing vibrational normal modes of a single molecule with atomically confined light," *Nature*, vol. 568, pp. 78–82, 2019.
[4] R. S. Alencar, C. Rabelo, H. L. S. Miranda, et al., "Probing Spatial Phonon Correlation Length in Post-Transition Metal Monochalcogenide GaS Using Tip-Enhanced Raman Spectroscopy," *Nano. Lett.*, vol. 19, pp. 7357–7364, 2019.
[5] T.-X. Huang, X. Cong, S-S. Wu, et al., "Probing the edge-related properties of atomically thin MoS_2 at nanoscale," *Nat Commun.*, vol. 10, pp. 5544, 2019.
[6] R. Zhang, Y. Zhang, Z. C. Dong, et al., "Chemical mapping of a single molecule by plasmon-enhanced Raman scattering," *Nature*, vol. 498, pp. 82–86, 2013.

[7] C. Lee, B. G. Jeong, S. J. Yun, Y. H. Lee, S. M. Lee, and M. S. Jeong, "Unveiling Defect-Related Raman Mode of Monolayer WS_2 via Tip-Enhanced Resonance Raman Scattering," *ACS Nano*., vol. 12, pp. 9982–9990, 2018.
[8] C. Chen, N. Hayazawa, and S. Kawata, "A 1.7 nm resolution chemical analysis of carbon nanotubes by tip-enhanced Raman imaging in the ambient," *Nat. Commun*., vol. 5, p. 3312, 2014.
[9] K.-D. Park, M. B. Raschke, J. M. Atkin, Y. H. Lee, and M. S. Jeong, "Probing Bilayer Grain Boundaries in Large-Area Graphene with Tip-Enhanced Raman Spectroscopy," *Adv. Mater*., vol. 29, p. 1603601, 2017.
[10] K.-D. Park, T. Jiang, G. Clark, X. Xu, M. B. Raschke, "Radiative control of dark excitons at room temperature by nano-optical antenna-tip Purcell effect," *Nat. Nanotechnol*., vol. 13, pp. 59–64, 2018.
[11] *Optical Antennas*. Cambridge: Cambridge University Press, 2013.
[12] L. Novotny, N. van Hulst, "Antennas for light," *Nat. Photonics*., vol. 5, pp. 83–90, 2011.
[13] T. L. Vasconcelos, B. S. Archanjo, B. Fragneaud, et al. "Tuning Localized Surface Plasmon Resonance in Scanning Near-Field Optical Microscopy Probes," *ACS Nano*., vol. 9, pp. 6297–6304, 2015.
[14] T. Hibi, K. Ishikawa, "Study of Point Cathode by Using Müller's Type Microscope," *J Electron Microsc*., vol. 9, pp. 13–15, 1960.
[15] G. Binnig, H. Rohrer, C. Gerber, E. Weibel, "Surface Studies by Scanning Tunneling Microscopy," *Phys. Rev. Lett*., vol. 49, pp. 57–61, 1982.
[16] Y. K. Cheong, K. S. Lim, W. H. Lim, W. Y. Chong, R. Zakaria, H. Ahmad, "Note: Fabrication of tapered fibre tip using mechanical polishing method," *Rev. Sci. Instrum*., vol. 82, p. 086115, 2011.
[17] C. Ropers, C. C. Neacsu, T. Elsaesser, M. Albrecht, M. B. Raschke, C. Lienau, "Grating-Coupling of Surface Plasmons onto Metallic Tips: A Nanoconfined Light Source," *Nano. Lett*., vol. 7, 2784–2788, 2007.
[18] S. S. Kharintsev, G. G. Hoffmann, A. I. Fishman, M. K. Salakhov, "Plasmonic optical antenna design for performing tip-enhanced Raman spectroscopy and microscopy," *J. Phys. D. Appl. Phys*., vol. 46, p. 145501, 2013.
[19] A. Dominget, J. Farkas, S. Szunerits, "Characterization of post-copper CMP surface with scanning probe microscopy: Part II: Surface potential measurements with scanning Kelvin probe force microscopy," *Microelectron Eng*., vol. 83, 2355–2358, 2006.
[20] T. W. Johnson Z. J. Lapin, R. Beams, et al., "Highly Reproducible Near-Field Optical Imaging with Sub-20-nm Resolution Based on Template-Stripped Gold Pyramids," *ACS Nano*., vol. 6, pp. 9168–9174, 2012.
[21] B. Ren, G. Picardi, B. Pettinger, "Preparation of gold tips suitable for tip-enhanced Raman spectroscopy and light emission by electrochemical etching," *Rev. Sci. Instrum*., vol. 75, pp. 837–841, 2004.
[22] C. Lee, S. T. Kim, B. G. Jeong, et al., "Tip-Enhanced Raman Scattering Imaging of Two-Dimensional Tungsten Disulfide with Optimized Tip Fabrication Process," *Sci. Rep*., vol. 7, p. 40810, 2017.
[23] P. Kim, J. H. Kim, M. S. Jeong, D.-K. Ko, J. Lee, S. Jeong, "Efficient electrochemical etching method to fabricate sharp metallic tips for scanning probe microscopes," *Rev. Sci. Instrum*., vol. 77, p. 103706, 2006.
[24] M. Lopes, T. Toury, M. L. de La Chapelle, F. Bonaccorso, P. Giuseppe Gucciardi, "Fast and reliable fabrication of gold tips with sub-50 nm radius of curvature for tip-enhanced Raman spectroscopy," *Rev. Sci. Instrum*., vol. 84, p. 073702, 2013.
[25] L. Billot, L. Berguiga, M. L. de la Chapelle, Y. Gilbert, R. Bachelot, "Production of gold tips for tip-enhanced near-field optical microscopy and spectroscopy: analysis of the etching parameters," *Eur. Phys. J- Appl. Phys*., vol. 31, pp. 139-145, 2005.
[26] S. S. Kharintsev, A. I. Noskov, G. G. Hoffmann, J. Loos, "Near-field optical taper antennas fabricated with a highly replicable ac electrochemical etching method," *Nanotechnology*., vol. 22, p. 025202, 2010.
[27] T. Ito, P. Bühlmann, Y. Umezawa, "Scanning Tunneling Microscopy Using Chemically Modified Tips," *Anal. Chem*., vol. 70, pp. 255–259, 1998.
[28] B. Yang, E. Kazuma, Y. Yokota, Y. Kim, "Fabrication of Sharp Gold Tips by Three-Electrode Electrochemical Etching with High Controllability and Reproducibility," *J. Phys. Chem. C*., vol. 122, pp. 16950–16955, 2018.
[29] S. Ye, C Ishibashi, K. Shimazu, K. Uosaki, "An In Situ Electrochemical Quartz Crystal Microbalance Study of the Dissolution Process of a Gold Electrode in Perchloric Acid Solution Containing Chloride Ion," *J. Electrochem. Soc*., vol. 145, 1998.
[30] D. R. Lide, "*CRC handbook of chemistry and physics*". CRC Press, 2004.
[31] L. W. Hanlon, M. Romaine, III, F. J. Gilroy, J. E. Deitrick, "Lithium chloride as a substitute for sodium chloride in the diet: Observations on Its Toxicity," *J. Am. Med. Assoc*., vol. 139, pp. 688–692, 1949.
[32] J. H. Talbott, "Use of lithium salts as a substitute for sodium chloride," *Arch. Intern. Med*., vol. 85, pp. 1–10, 1950.
[33] D. Gingery, P. Bühlmann, "Single-step electrochemical method for producing very sharp Au scanning tunneling microscopy tips," *Rev. Sci. Instrum*., vol. 78, p. 113703, 2007.
[34] N. Kumar, A. Rae, D. Roy, "Accurate measurement of enhancement factor in tip-enhanced Raman spectroscopy through elimination of far-field artefacts," *Appl. Phys. Lett*., vol. 104, p. 123106, 2014.